Techno-economic assessment of hydrogen selective membranes for CO_2 capture in integrated gasification combined cycle

Matteo Gazzani, Davide Maria Turi, Giampaolo Manzolini *

Politecnico di Milano, Dipartimento di Energia, Via Lambruschini 4, 20156 Milano, Italy

Received 28 May 2013
Received in revised form 3 October 2013
Accepted 12 November 2013
Available online 7 December 2013

1. Introduction

The increase of carbon dioxide concentration in the atmosphere with potential negative impact on the climate has driven the research activity towards CO_2 neutral technologies for power production. Besides renewable energy such as wind, solar, hydro, which produces electricity without any direct emissions, capturing CO_2 in fossil fuel based plant is the most recognized technol-ogy to limit the fossil fuel impact on the environment (DOE, 2007; International Energy Agency, 2008). Different routes can be employed in power plant for capturing CO_2. The first, also known as post-combustion capture, is based on capturing CO_2 in the exhaust gases. This configuration is regarded as the state-of-the-art process for CO_2 capture when based on conventional chemical absorption (Amrollahi et al., 2011; Rao and Rubin, 2002; Wang et al., 2011). Moreover, advanced technologies are under investigation to reduce the efficiency penalties of post-combustion capture (Chiesa et al., 2011; Riberiro et al., 2012; Valenti et al., 2012).

The second route option consists of oxygen combustion: the flue gases are a mixture of CO_2 and steam and almost pure CO_2 is obtained after the water condensation. Nevertheless, further gas conditioning steps are required to cope with inert and pollutants contamination (White et al., 2010).

The last option is the pre-combustion decarbonisation which implies transferring the carbon-bounded energy content from fuel (either coal or natural gas) to hydrogen; this is then burned in a combined cycle, producing power without any CO_2 emission. In case of natural gas fuelled plant, pre-combustion configuration requires a reforming section to convert methane into hydrogen (Nord et al., 2009; Romano et al., 2010). When the plant feed-stock is coal, as in this work, the pre-combustion technology suits very well into integrated gasification combined cycles (IGCC). In IGCC, coal is firstly converted into syngas thanks to a gasifier reactor; the gasification pressure can be equal to 40 bar, if Shell-Prenflo gasifier is assumed (Franco et al., 2011, 2010; Gazzani et al., 2013a,b), or 70 bar with GE's technology (DOE/NETL-2011/1498, n.d.). The obtained, clean syngas is then utilized in a combined cycle.

In addition to the capture route, there are several technologies available for CO_2 separation. As far as pre-combustion is concerned, the conventional ones are based on commercial acid gas removal (AGR), (i.e. Rectisol™, Selexol®, Sulfinol®) with the separation of the CO_2 together with H_2S (DOE/NETL-2011/1498, n.d.; Franco et al., 2010). These technologies introduce significant efficiency penalties as well as additional equipment. Accordingly, advanced CO_2 separation processes are under investigation with the aim of reducing both economic and performance penalties. Examples of

* Corresponding author. Tel.: +39 0223993810; fax: +39 0223993913.
E-mail address: giampaolo.manzolini@polimi.it (G. Manzolini).

Nomenclature and acronyms

AGR	acid gas removal
ASU	air separation unit
BOP	balance of plant
BUA	bottom-up approach
CCR	carbon capture ratio [%]
CCS	carbon capture and storage
COT	combustor outlet temperature [°C]
DLN	dry low NO_x
E	CO_2 emission rate [kg_{CO_2}/kWh_{el}]
EBTF	European Benchmark Task Force
EPC	engineering, procurement and construction
EXP	expansion
HR	heat rate [kJ_{LHV}/kWh_{el}]
HRF	hydrogen recovery factor
HRSC	heat recovery steam cycle
HRSG	heat recovery steam generator
GT	gas turbine
IC	indirect cost
IGCC	integrated gasifier combined cycle
LP	low pressure
OBL	outside battery limits
O&M	operation and maintenance
PF	post firing
SEWGS	sorption enhanced water gas shift
SH	super heating
SPECCA	specific primary energy consumption for CO_2 avoided [MJ_{LHV}/kg_{CO_2}]
TDPC	total direct plant cost [M€]
TIT	turbine inlet temperature (total temperature ahead of the first rotor) [°C]
TIT_{iso}	turbine inlet temperature (defined according to ISO standard) [°C]
TOT	turbine outlet temperature [°C]
TPC	total plant cost [M€]
WGS	water gas shift
WGSR	water gas shift reactor

Subscripts

El	electrical
REF	reference

Greek symbols

η	efficiency [%]

innovative technologies are low temperature sorbents (Casas et al., 2012; Schell et al., 2013), high temperature sorbents integrated in water gas shift reactors usually named SEWGS (Dijk et al., 2011; Manzolini et al., 2013) calcium looping (Martinez et al., 2013) and membranes (Anantharaman and Bolland, 2011; Bredesen et al., 2004; Chiesa et al., 2007; Scholes et al., 2010). The latter have long attracted the attention of the research community. The reason behind this wide investigation is in the simplicity of membranes, which can separate different gas components through a continuous process.

CO_2 capture can be achieved through different kind of membranes as they can be selective to either Oxygen, Hydrogen or CO_2. This work focuses on the application of hydrogen selective Pd-based membranes to IGCC plants. In particular, the selected gasification technology is based on Shell-Prenflo gasifier which guarantees very high cold gas efficiency (Grabner and Meyer, 2013; Higman and van der Burgt, 2008). There is a significant number of publications available in literature about Pd-based membranes for CO_2 capture (Chiesa et al., 2007; De Lorenzo et al., 2008; Jordal et al., 2004; Ku et al., 2011; Lee et al., 2013; Nord et al., 2009; Schiebahn et al., 2012), even if most of these publications are about membrane applications in NGCC plants; this is because the NG is a sulphur free fuel and Pd-membranes cannot withstand sulphur concentrations above the 10 ppm-level, hence requiring an AGR process upstream.

Compared to previous studies already available in literature, this work brings significant improvements:

- Each component of the power plant, as the gasification island, the power section and the hydrogen separation is modelled in detail. The model used was calibrated with experimental data and real performance.
- Membrane module costs are based on a detailed design performed in CACHET-II project together with partners. Moreover, two different type of membranes are discussed (Peters et al., 2012; Song and Forsyth, 2013; Van Berkel et al., 2013).
- Innovative lay-outs are introduced taking into account the peculiarity of the syngas composition; all the lay-outs are evaluated on the base of EBTF methodology (Franco et al., 2011, 2010), making them consistent with all EU projects on CO_2 capture.
- The optimization is performed in economic terms minimizing the cost of CO_2 avoided. Several membrane operating conditions are evaluated to determine the optimal configuration.

2. Membranes: principles and concepts for CO_2 capture in IGCC

Hydrogen selective membranes are recognized as a promising technology for reducing efficiency penalty in power plants with CO_2 capture (Beavis, 2011). Among different membrane technologies (Bredesen et al., 2004), the hydrogen selective one perfectly fits in the precombustion decarbonization concept (Jordal et al., 2004; Mejdell et al., 2009). In particular, Pd-based membranes are among the most investigated thanks to their high H_2 selectivity and good hydrogen fluxes. Moreover, hydrogen separation is performed at medium temperature (350–500 °C) allowing for membrane inte-gration in the WGS process, and for the direct use of the separated hydrogen as fuel for the gas turbines (Chiesa et al., 2007). Weak points which have to be improved are: (i) the tolerance to sulphur and (ii) the stability. In addition, the membrane behaviour in CO rich conditions must be investigated more in detail.

Two different kinds of membranes were developed in CACHET-II project and both are considered in this work: the first is a pure Pd membrane showing a high H_2 permeance, but no tolerance towards sulphur. The second is a Pd-alloy based membrane which has a reduced permeance but can support sulphur content up to 1–2 ppm without reducing the flux to a large extent (Peters et al., 2012). Since the sulphur content in the syngas is in the range of 5000–10,000 ppm, a sulphur removal system upstream the membrane is required.

Usually, when hydrogen selective membranes are considered for CO_2 capture in power plants, the membrane reactor concept is adopted. Membrane reactor consists of simultaneous hydrogen conversion and separation; in the IGCC plant case, membranes are integrated with the water gas shift reaction. Driven by techno-economic assessment and plant operation issues carried out in CACHET 2 project, membrane separator modules were chosen instead of membrane reactors (i.e. no WGS reaction is performed together with the hydrogen separation) (Song and Forsyth, 2013; Van Berkel et al., 2013). For example, given the limited membrane life time, module substitution is much easier when no catalyst is present. Moreover, the adoption of membrane modules instead of

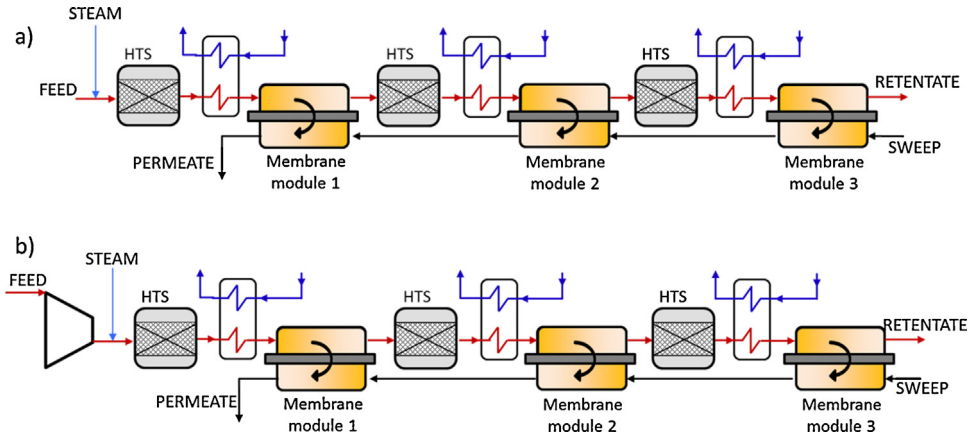

Fig. 1. Membrane separation concept adopted in CACHET-II: (a) three membrane modules with working pressure defined by the gasification island. (b) Three membrane modules with compression of the feed stream.

membrane reactors reduces temperature variation issues caused by WGS reaction inside and along the membranes. Otherwise significant temperature gradients (>50–100 °C) can occur inside the reactor with detrimental impact as consequence of the different thermal expansion between the membrane layer and the porous support.

The membrane separator concept is based on membrane modules, which can be even two or three in series, with adiabatic high temperature shift (HTS) reactor in between to increase the CO conversion (Middleton et al., 2005). The number of HTS depends on the amount of hydrogen to be separated, also known as Hydrogen Recovery Factor (HRF). When HRF lower than 90% is considered, only one HTS can be adopted, while for higher HRF (>90%) additional HTS are required in order to convert as much CO as possible. The hydrogen separation concept developed in CACHET-II is shown in Fig. 1.

In order to limit the membrane area, different values of working pressure were investigated; as the gasification pressure cannot be changed, compression of the feed stream was considered. This effect will be deeply discussed in the following sections. Moreover it must be recalled that the permeate pressure is set to guaran-tee the required fuel injection pressure inside the Gas Turbine (GT) combustor (25 bar). This results in a lower membrane driving force compared to the ambient pressure permeate. On the other hand the plant layout is simpler and more efficient. Paragraph 4.2 will describe an innovative solution which tries to encompass the abovementioned limit.

3. Effects of gasification process on membrane integration

Among coal based power plants, IGCC was selected as the most suitable for hydrogen-selective membrane application: thanks to the high pressure syngas, the hydrogen permeation across the membrane is enhanced. After a preliminary comparison of different gasification technologies (Manzolini et al., 2011), the Shell dry feed process was selected. The adoption of a dry feed gasifier with high carbon conversion (>99%) leads to higher gasifier efficiency (measured in terms of cold gas efficiency), when compared to slurry fed gasifiers. The main drawback of this technology when applied to a membrane-integrated process is the significant inert concentration in the syngas, mostly nitrogen used as fuel carrier. This reduces (i) the H_2 partial pressure in the membrane feed and consequently lower H_2 fluxes through the membrane and (ii) the CO_2 purity after the hydrogen separation. If the CO_2 concentration limits before sequestration are not satisfied, an additional purification step must be introduced. According to EBTF guidelines (Franco et al., 2011, 2010; Manzolini et al., 2012a,b) the volumetric concentration of inert gases is limited to 4% which can be hardly met when lock-hopper feeding process is adopted (e.g. like in the Shell gasifier).

These issues can be solved in two ways:

- Adopting a retentate purification step whose energy and cost penalties are limited. This is the most conservative solution as it does not affect the gasification island. Nevertheless, it does not cope with the decrease of the hydrogen partial pressure.
- Modifying the coal feeding system of the gasifier preventing nitrogen dilution. This option increases both the CO_2 purity and the specific power output. As drawback, it requires modifications of the gasification process which can be critical.

The first solution leads to the adoption of a cryogenic purification system. Such a process can reduce the energy consumption for purification of CO_2-rich streams when the initial CO_2 concentration is higher than about 60% (Chiesa et al., 2011).

The second solution leads to the adoption of CO_2 as coal feeding carrier inside the lock hopper (Guo et al., 2012). As abovementioned, this is not a commercial solution and it requires making some assumptions in order to evaluate the potentiality. Also in this case an additional step downstream the membrane section would be required to recovery the hydrogen-linked energy remaining in the retentate. Thanks to the negligible amount of diluents (N_2 + Ar), an oxycombustion of the retentate could be carried out. A future work will deal on the adoption of CO_2 feeding. A schematic of the two concepts with the main compositions and adopted purification processes is shown in Fig. 2.

3.1. Cryogenic CO_2 purification

As cryogenic process, two different concepts are available: (i) the conventional external chillers based configuration and (ii) the internal refrigerating configuration. The first solution has benefits from an efficiency point of view: the lower energy requirement compared to the internal cycle is about 10% when ethane is used as cooling media (Manzolini et al., 2012a,b) and 4% with ethylene. On the other hand, the internal refrigerating configuration requires less equipment reducing investment and make-up costs. The absolute energy consumption difference is about 1MW which is negligible in the overall power balance and which makes the cheaper self-refrigerated configuration the preferred one. This decision was supported by industrial partner of CACHET-II consortium.

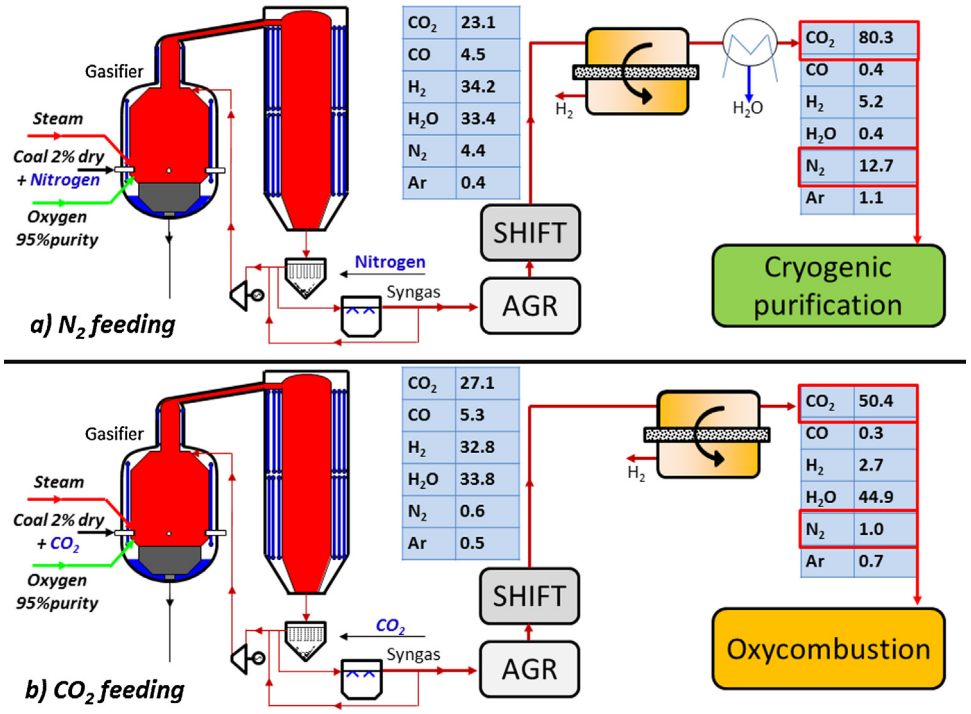

Fig. 2. Schematic of the gasification and hydrogen separation section for HRF = 95%; (a) gasifier with nitrogen as coal carrier and (b) gasifier with CO_2 as coal carrier.

The cryogenic CO_2 purification consists of a self-refrigerated system which uses the CO_2 separated as cooling source. It is based on two-steps flash separation which reduces the compression power required to overcome the process pressure losses. This concept is comprehensively discussed in (Chiesa et al., 2011, 2007) and a brief description is proposed here.

In the adopted configuration, the CO_2-rich stream is firstly dehydrated with a circulating triethylene glycol desiccant and/or molecular sieve to prevent plugging due to ice formation in the cold section.

The stream is then cooled and partially condensed in a multi-flow heat exchanger. The temperature of the CO_2 stream at the outlet of this heat-exchanger is an important parameter in operating the process. The optimal temperature has been set around −30 °C, a value that minimizes the overall compression power. Note also that the extent to which incondensable gases can be recovered is almost independent of the temperature.

The liquid separated in the first knockout drum is throttled through valve and used as cold stream in the multi-flow heat exchanger. Since the separation efficiency increases monotonically with decreasing temperature, the vapor fraction exiting the first knockout drum is further cooled down to −53 °C through the two additional exchangers. This value, which was adopted also in a pre-vious work (Berstad et al., 2013), has been selected to ensure that the temperature of the stream remains slightly above (+0.6 °C) the CO_2 freezing point. The liquid streams separated in the drums and evaporated in the heat exchangers are finally mixed, compressed in an intercooled compression train up to 80 bar and then pumped in liquid phase to 110 bar for long range transportation. Accord-ing to calculation carried out, the CO_2 separation efficiency ranges between 95% and 98% whilst the CO_2 stream purity is in between 96% and 98% (mol basis).

The vapor fraction with incondensable and part of the CO_2 is sent to the gas turbine along with the hydrogen/nitrogen mixture. It contains almost 96% of the original LHV value of the input stream, which means that about 4% of H_2 and CO at the inlet of the cryogenic system is dissolved in the liquid CO_2. The vapor fraction represents about 9% of the total fuel input to the gas turbine (LHV basis).

4. Lay-out discussion

All membrane modules discussed are integrated in an IGCC, coal based, plant. As already anticipated, the gasification technology is based on Shell–Prenflo dry feed gasifier. The power and mass bal-ances of the gasifier were provided by Shell within the European Benchmark Task Force (Franco et al., 2010).

4.1. Base case configuration

As shown in Fig. 3, the process is equal to the reference IGCC case without CO_2 capture until the AGR; this allows the obtained results to be consistent with the reference cases (Franco et al., 2010; Gazzani et al., 2013a,b). CO shift conversion is carried out after the sulphur removal section reducing CO_2 venting in AGR and steam condensation exergy losses. The gasification pressure is set at 44 bar, as indicated by Shell, this is a trade-off between efficiency, which takes advantage of low pressure, and gasifier size. Considering the sulphur tolerance of the two membranes, two AGR processes have been considered: Rectisol for pure Pd membrane and Selexol for the Pd-alloy based membranes, which can toler ate H_2S up to 5 ppm. The Selexol process is based on a mixture of dimethyl ethers of polyethylene glycol, while Rectisol is based on chilled methanol (Korens et al., 2002). From an overall point of view, Rectisol and Selexol differently affect the plant lay-out because of the COS removal: Rectisol is selective to H_2S and COS, while Selexol is more selective to H_2S requiring the upstream[1] conversion of COS. The power plant size is based upon one gasification train generating syngas for one gas turbine combined cycle. Oxygen is produced in an ASU partially integrated to the gas turbine compressor: 50% of the air at the ASU distillation column comes from the GT compressor. An expander between the gas turbine compressor and the ASU is adopted to decouple the pressures and recover part of the compression work. This configuration

[1] Selexol can capture COS as well, but the CO_2 co-captured would be significant with penalties for the CO_2 emissions.

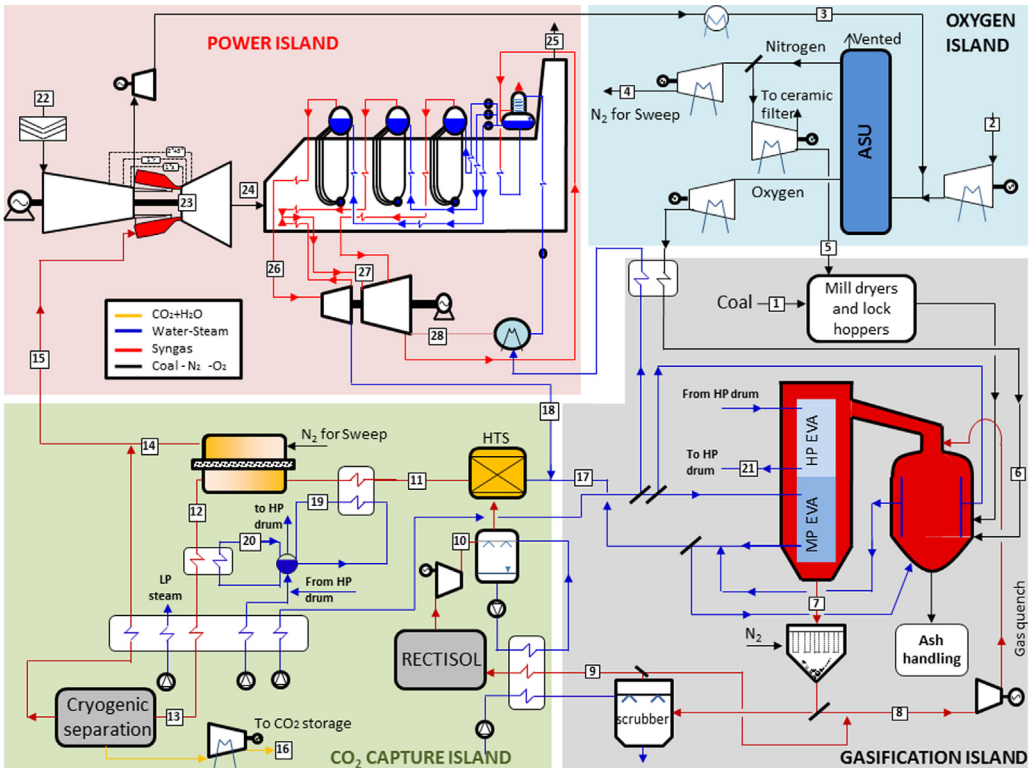

Fig. 3. Layout of the IGCC with capture through not sulfur tolerant membranes. Sulfur removal is based on Rectisol process; hydrogen recovery after membrane separation is carried out with cryogenic purification. Four macro areas are identified: air separation unit in light blue, Shell gasification process in light grey, CO_2 capture section in light green and power production in light red. (For interpretation of the references to color in this figure legend, the reader is referred to the web version of this article.)

was proposed as reference from the EBTF (Franco et al., 2011, 2010). N_2 produced in the ASU is compressed and used partly in lock hoppers for coal feeding and partly sent to the membrane modules as sweep gas, thus reducing the hydrogen partial pressure and leading to a decrease in membrane surface area required. Moreover, nitrogen is used in diffusive flame GT combustor to decrease the stoichiometric flame temperature and cope with NO_x formation (DLN combustors for hydrogen GT are not available yet). Syngas exits the scrubber at about 170 °C and then is further cooled to ambient temperature. In Selexol case, a catalytic bed for COS hydrolysis is placed. Low temperature heat is recovered producing hot water for the saturator. Syngas is then further cooled with water and sent to acid gas removal (AGR) unit after condensate separation.

After the AGR unit, syngas is saturated and additional steam is added in order to achieve 2.0 S/CO ratio at WGS. Saturator allows increasing water content in the syngas, which is generated by recovering low-temperature heat, and reducing the amount of required steam. The additional steam to achieve the 2.0 S/CO target comes from the IP steam generated in the gasification island and from the steam turbine at high pressure section outlet (usually named cold RH). The opportunity of compressing the syngas from 40 bar to about 60 bar before the saturator is also evaluated; higher syngas total pressure increases H_2 permeation driving force reducing the membrane surface area.

Both in Pd and in Pd-alloy membrane cases, the maximum membrane temperature is set at 400 °C (Guazzone and Ma, 2008; Peters et al., 2009). Since there is no reaction occurring in the module, the maximum temperature coincides with the feed inlet temperature, while at the outlet, the temperature is slightly lower because of the cooling effect of the sweep gas. This assumption affects mainly the membrane surface area rather than system efficiency since the fuel temperature at combustor inlet is set at 350 °C and also the retentate has to be cooled.

Three different HRF (90%, 95% and 98%) are assumed in order to outline its influence over electric efficiency and CO_2 capture ratio. The number of membrane modules in series for the hydrogen permeation (which can vary from 1 to n) will be optimized taking into account its impact in terms of membrane surface area.

As sweep gas, it is used nitrogen from ASU which is compressed to 25 bar with an intercooled compressor. The amount of sweep gas is set in order to have a H_2 concentration of 40% at reactor outlet. From a theoretical point of view, lowering the hydrogen content results in a lower membrane surface area required. Nevertheless a lower bound limit is set by the syngas LHV: commercial combustors for low calorific fuel combustion require at least 4000 kJ/Nm^3. After hydrogen separation, the retentate stream, which mainly consists of CO_2, H_2O and unconverted H_2 and CO, is cooled down to ambient temperature producing high pressure steam for the HRSG and IP water economization. Because of the high steam content and pressure, a part of condensation heat can be recovered for water economization (dew point is at about 200 °C).

As anticipated in the introduction section, the inert content in the CO_2 is significant. At 35 °C, CO_2 molar concentration, volume dry, is 76% and 82% at 90% and 98% of HRF respectively. In order to achieve a CO_2 purity above 96% and recover most of hydrogen and carbon monoxide, a cryogenic separation process has been adopted. The cryogenic process has a CO_2 separation efficiency, also called CO_2 capture ratio in the range of 90–95%, depending on the CO_2 purity at the inlet of the process, which is function of HRF. Detailed energy and mass balances for the reference membrane case with HRF = 95% is shown in Table 1.

4.2. *Post-firing configuration*

In addition to the previous configuration, where all the hydrogen separated in the membranes is burned in the GT combustor, a second lay-out is discussed here. In this new configuration, shown

Table 1
Mass, molar and energy balance for the main points labelled in Fig.3 (IGCC with not sulfur tolerant membranes).

Point	T °C	P bar	G kg/s	Q kmol/s	Ar	CO	CO_2	H_2	H_2O	H_2S	N_2	O_2
					Molar fraction [%]							
1	15.0	44.0	38.0	2.33				Douglas as in Table 3				
2	15.0	1.0	69.7	2.41	0.92	–	0.03	–	1.03	–	77.28	20.73
3	30.0	5.8	69.5	2.41	0.92	–	0.03	–	0.74	–	77.51	20.80
4	252.8	25.0	82.1	2.93	–	–	–	–	–	–	100.00	–
5	80.0	48.0	6.5	0.23	–	–	–	–	–	–	100.00	–
6	180.0	48.0	33.4	1.04	3.09	–	–	–	–	–	1.91	95.00
7	300.0	41.1	131.9	6.20	0.86	56.72	2.91	26.25	4.90	0.18	8.17	–
8	200.0	41.1	56.5	2.67	0.79	52.24	2.68	24.17	11.30	0.16	8.65	–
9	157.5	41.1	88.2	4.20	0.77	50.57	2.59	23.40	14.13	0.16	8.37	–
10	72.5	54.0	76.9	3.59	0.89	59.10	2.72	27.35	0.14	–	9.79	–
11	497.2	52.9	156.8	8.02	0.40	4.53	23.13	34.15	33.41	–	4.38	–
12	400.0	52.4	151.2	5.23	0.61	0.42	42.00	5.51	44.73	–	6.72	–
13	99.4	50.8	110.1	2.95	1.09	0.75	74.51	9.77	1.95	–	11.91	–
14	341.6	25.0	110.4	6.98	–	–	–	40.00	18.01	–	41.99	–
15	328.4	25.0	126.6	7.73	0.30	0.24	1.75	39.68	16.28	–	41.74	–
16	50.0	50.3	92.9	2.15	0.42	0.17	96.00	0.71	–	–	2.71	–
17	147.5	53.5	82.7	3.91	0.82	54.26	2.50	25.11	8.32	–	8.98	–
18	393.1	54.0	74.1	4.11	–	–	–	–	100.00	–	–	–
19	337.0	144.0	38.1	2.11	–	–	–	–	100.00	–	–	–
20	343.0	144.0	9.3	0.52	–	–	–	–	100.00	–	–	–
21	345.0	144.0	100.1	5.56	–	–	–	–	100.00	–	–	–
22	15.0	1.0	608.1	21.08	0.92	–	0.03	–	1.03	–	77.28	20.73
23	1440.0	17.6	525.7	20.02	0.75	–	0.79	–	22.32	–	69.52	6.62
24	603.1	1.0	665.0	24.85	0.79	–	0.64	–	18.18	–	71.03	9.36
25	115.0	1.0	665.0	24.85	0.79	–	0.64	–	18.18	–	71.03	9.36
26	559.2	133.9	168.5	9.35	–	–	–	–	100.00	–	–	–
27	559.1	44.3	107.7	5.98	–	–	–	–	100.00	–	–	–
28	32.2	0.0	112.9	6.27	–	–	–	–	100.00	–	–	–

in Fig. 4, the overall membrane section is divided into two macro areas. In the first zone, which is composed by three membrane modules, hydrogen is separated at the pressure required by the GT combustor while in the second zone, hydrogen is separated at ambient pressure and used to post-fire the heat recovery steam generator. The most part of H_2, 90% of the total separated, is still sent to the GT combustor; different hydrogen repartition to the GT or post-firing is considered in a sensitivity analysis. The rationales behind this second configuration are: (i) the membrane surface area can be extremely large if all the hydrogen is separated at high pressure and (ii) the integration of the heat available from the gasification island and the HRSG makes the heat recovery not efficient (see detailed discussion in the result section). In particular, the gasification island produces a large mass flow of saturated steam (both at high and medium pressure) which has to be pre-heated and super-heated in the HRSG. This penalizes the heat transfer because there is lack of heat available at low and high temperature.

It is important to stress that this new configuration does not feature any technology barrier: post-firing is widely adopted in combined cycle and CACHET-II membrane can stand up to 100 bar of absolute pressure difference (Van Berkel et al., 2013).

The resulting lay-out is presented in Fig. 5. The only difference with the previous one is that there are two different hydrogen streams produced: 90% of the separated hydrogen is diluted with nitrogen at 25 bar and sent to the gas turbine. The remaining, slightly diluted with nitrogen, is obtained at 1.1 bar, and is used to post-fire the heat recovery steam generator. Detailed energy and mass balances for the post-firing layout case with HRF = 90% are shown in Table 2.

5. Model description and assumptions

This section discusses the modelling approach and assumptions adopted to simulate the power cycles presented in the previous chapter. Main assumptions are summarized in Table 3. Mass and energy balances have been estimated by a proprietary computer code (GS) developed by the GECoS group at the Department of Energy of the Politecnico di Milano to assess the performance of gas/steam cycles, CO_2 capture systems, as well as a variety of other plant options, including IGCC, membranes, etc. (Chiesa and Macchi, 2004; Lozza, 1990; Macchi et al., 1995). The plant scheme is reproduced by assembling in a coherent network the different components selected in a library containing over 20 basic modules,

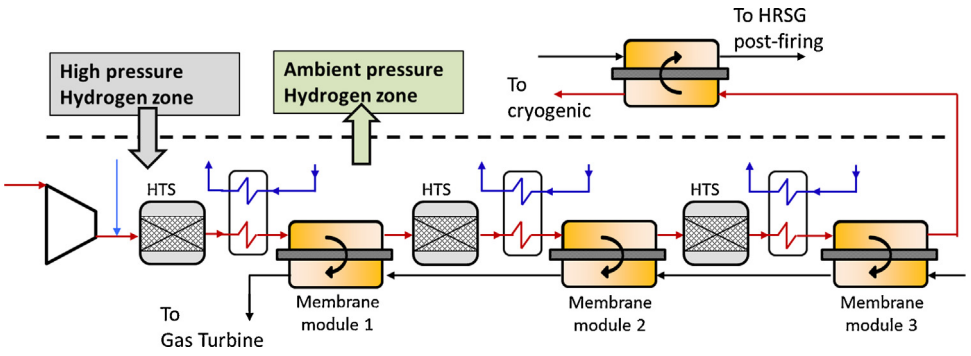

Fig. 4. Membrane module layout for combined GT and HRSG post-firing hydrogen production.

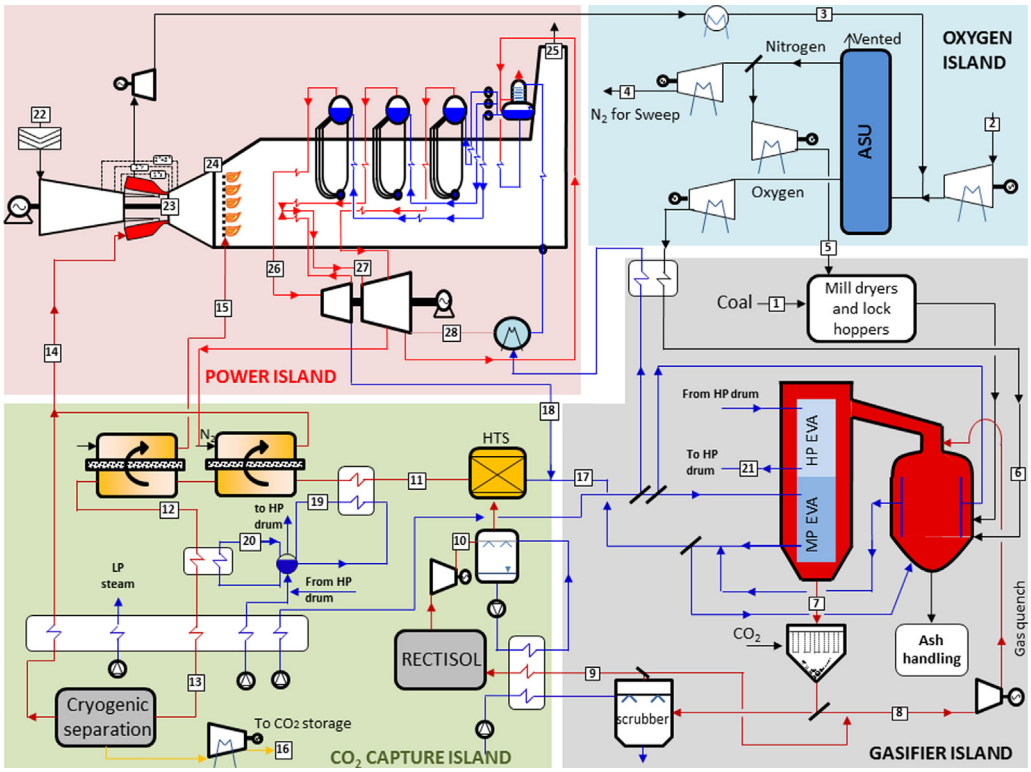

Fig. 5. Layout of the IGCC with capture through not sulfur tolerant membranes. Sulfur removal is based on Rectisol process; hydrogen recovery after membrane separation is carried out with cryogenic purification. HRSC features the post-firing of flue gas with hydrogen separated at ambient pressure.

whose models have been previously implemented. Built-in rules for efficiency prediction of turbomachines (gas and steam turbine, compressors), as a function of their operating conditions, as well as built-in correlations for predicting gas turbine cooling flows allow the code to generate very accurate estimations of combined cycles performance, even for off-design conditions. The gas turbine model in GS is calibrated to correctly predict the performance of advanced gas turbines, accounting for all the relevant phenomena occurring: fluid-dynamic losses, cooling circuit performance, changes in gas turbine fuel and working fluid composition. The model is 1-D and

Table 2
Mass, molar and energy balance for the main points labelled in Fig.5 (IGCC with not sulfur tolerant membranes + HRSC post-firing).

Point	T	P	G	Q	Ar	CO	CO_2	H_2	H_2O	H_2S	N_2	O_2
	°C	bar	kg/s	kmol/s	Molar fraction [%]							
1	15.0	44.0	41.2	2.52	Douglas as in Table 3							
2	15.0	1.0	75.4	2.61	0.92	–	0.03	–	1.03	–	77.28	20.73
3	30.0	5.8	75.3	2.61	0.92	–	0.03	–	0.74	–	77.51	20.80
4	252.8	25.0	88.1	3.14	–	–	–	–	–	–	100.00	–
5	80.0	48.0	7.1	0.25	–	–	–	–	–	–	100.00	–
6	180.0	48.0	36.1	1.12	3.09	–	–	–	–	–	1.91	95.00
7	300.0	41.1	142.7	6.71	0.86	56.75	2.90	26.26	4.88	0.18	8.17	–
8	200.0	41.1	61.0	2.89	0.79	52.26	2.67	24.18	11.28	0.16	8.65	–
9	157.5	41.1	95.5	4.54	0.77	50.59	2.58	23.41	14.11	0.16	8.37	–
10	73.7	54.6	83.3	3.89	0.89	59.11	2.71	27.35	0.14	–	9.78	–
11	497.7	53.5	155.6	7.90	0.44	6.12	24.32	36.45	27.86	–	4.82	–
12	400.0	50.8	149.6	4.95	0.70	2.28	46.28	6.06	36.99	–	7.69	–
13	113.1	49.3	118.5	3.22	1.08	3.51	71.07	9.30	3.22	–	11.80	–
14	322.5	25.0	129.5	7.54	0.35	1.29	2.24	39.00	11.10	–	46.02	–
15	359.1	1.2	1.6	0.33	–	–	–	89.21	–	–	10.80	–
16	50.0	48.8	95.7	2.21	0.38	0.71	95.85	0.60	–	–	2.45	–
17	144.0	54.0	88.9	4.20	0.83	54.76	2.51	25.34	7.48	–	9.06	–
18	388.4	54.0	66.7	3.70	–	–	–	–	100.00	–	–	–
19	337.3	144.0	25.8	1.43	–	–	–	–	100.00	–	–	–
20	343.0	144.0	8.9	0.49	–	–	–	–	100.00	–	–	–
21	345.0	144.0	108.4	6.02	–	–	–	–	100.00	–	–	–
22	15.0	1.0	611.0	21.18	0.92	–	0.03	–	1.03	–	77.28	20.73
23	1439.7	17.6	528.3	19.85	0.77	–	1.37	–	19.76	–	71.32	6.78
24	601.8	1.0	665.0	24.59	0.80	–	1.11	–	16.15	–	72.47	9.47
25	115.0	1.0	666.6	24.77	0.80	–	1.10	–	17.22	–	72.07	8.81
26	559.2	133.9	195.2	10.84	–	–	–	–	100.00	–	–	–
27	559.1	44.3	142.8	7.93	–	–	–	–	100.00	–	–	–
28	32.2	0.0	138.3	7.68	–	–	–	–	100.00	–	–	–

Table 3
Ambient conditions, fuel characteristics and main component assumptions (Franco et al., 2011, 2010).

Ambient conditions	15 °C/1.013 bar/60% RH			
Air composition, dry molar fraction (%)	N_2 78.08%, CO_2 0.04%, Ar 0.93%, O_2 20.95%			
Douglas Premium coal characteristics	C	66.52%	O	5.46%
Ultimate	N	1.56%	Clorine	0.009%
analysis	H	3.78%	Moisture	8.0%
	S	0.52%	Ash	14.15%
Coal LHV, HHV	25.17 MJ/kg, 26.23 MJ/kg			
CO_2 specific emission	349.0 [g/kWhLHV]			

Gas turbine	
Pressure ratio	18.1
Gas mass flow rate at the turbine inlet	650 kg/s
TIT	1360 °C
Pressure loss at inlet	1 kPa
Heat recovery steam cycle [HRSC]	
Pressure levels, bar	144, 54, 4
Maximum temperature SH e RH	565 °C
Pinch, subcooling, approach ΔT	10/5/25 °C
Condensing pressure	0.048 bar (32 °C)
Turbine Isentropic efficiency (HP/IP/LP)	92/94/88%
Pumps efficiency	70%
HRSG thermal losses	0.7% of thermal input
HRSG pressure losses, gas side	4 kPa
Gas turbine and steam cycle	
Generator efficiency	98.7%
Mechanical efficiency	99.6%
Power consumed for heat rejection	0.8% of heat released
Air separation unit	
Oxygen purity	95%
Nitrogen purity	99%
Oxygen outlet temperature	20 °C
Oxygen temperature entering the gasifier	180 °C
Oxygen pressure entering the gasifier	48 bar
Oxygen and nitrogen temperature leaving ASU	22 °C
Gasification section	
Gasifier outlet pressure	44 bar
Gasifier outlet temperature	1550 °C
Coal conversion	99.3%
Heat to membrane walls [% of thermal input LHV]	0.9%
O/C ratio	0.44
Dry quench exit temperature	900 °C
Scrubber inlet temperature	298 °C
Selexol process (H_2S removal)	
Electrical energy consumption	0.538 kWh/kg_{H_2S}
Thermal energy consumption	5.82 kWh/kg_{H_2S}
CO_2 venting	1.42 mol CO_2/mol H_2S
Rectisol process (H2S removal)	
Electrical energy consumption	7.49 kWh/kg_{H_2S}
Thermal energy consumption	16.72 kWh/kg_{H_2S}
CO_2 venting	6.62 mol CO_2/mol (H_2S+COS)
CO_2 separation and compression	
Final delivery pressure	110 bar
Compressor isentropic efficiency	85%
Temperature for CO_2 liquefaction	25 °C
Pressure drop for intercoolers and dryer	1.0%
Pump efficiency	75%
CO_2 purity	>96%

capable of calculating the blade coolant flow depending on expanding gas composition, thus, the same TIT of NG case can be assumed (i.e. compared to NG applications, coolant flow for IGCC increases from 17% to 23% of air compressor inlet). The gas turbine simulated is a generic "F Class" and its calibration was already discussed in (Manzolini et al., 2012a,b). All the assumptions, when available, are consistent with the EBTF report.

About Rectisol and cryogenic CO_2 separation, which are not considered in EBTF, detailed simulations were performed in Aspen Plus®.

Two important parameters that significantly affect the system performance are the fuel temperature and pressure at the inlet of the gas turbine combustor. A 5 bar overpressure on the air is assumed, while a fuel temperature of 350 °C is taken as reference. Avoiding fuel cooling and assuming a fuel temperature of 400 °C, the efficiency gain would be of 0.1% point. The same absolute efficiency variation, but negative in value, can be extended for lower fuel temperatures.

The results of the thermodynamic simulations are expressed in terms of (net electrical LHV) efficiency and CO_2 capture ratio, given respectively by:

$$\eta_{el} = \frac{\text{Net power}}{\text{Thermal power input } (\text{LHV}_{NG})} \quad (1)$$

$$\text{CCR} = \frac{\text{CO}_2 \text{ captured}}{\text{max amount CO}_2 \text{ produced from fuel used}} \quad (2)$$

Finally, a measure of the energy cost related to CO_2 capture is given by the specific primary energy consumption for CO_2 avoided

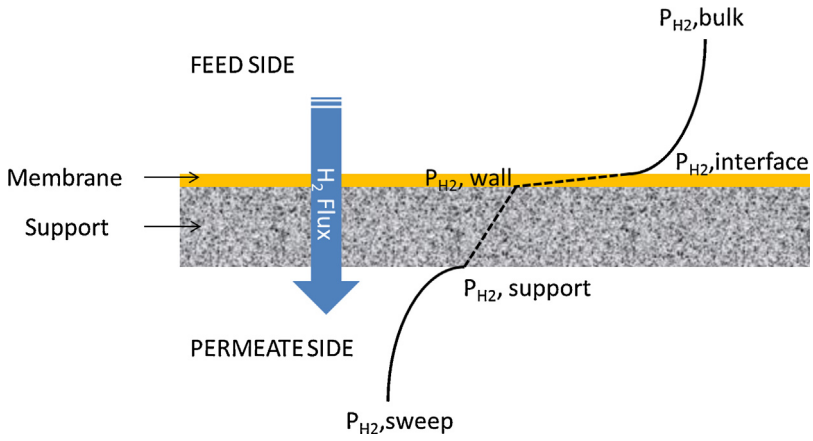

Fig. 6. Hydrogen mass transfer modelling across the membrane.

(SPECCA), already introduced in (Campanari et al., 2010), which is defined as:

$$\text{SPECCA} = \frac{\text{HR} - \text{HR}_{\text{REF}}}{E_{\text{REF}} - E} = \frac{3600 \cdot \left(\frac{1}{\eta} - \frac{1}{\eta_{\text{REF}}}\right)}{E_{\text{REF}} - E} \quad (3)$$

where:

- HR is the heat rate of the plant, expressed in kJ_{LHV}/kWh_{el}
- E is the specific CO_2 emission rate, expressed in kg_{CO_2}/kWh_{el}
- REF is the reference case for electricity production without carbon capture.

Special attention must be focused on the membrane modelling because of its significant impact on the results presented in this work.

The membrane surface area was determined with a two-dimensional model developed by SINTEF within the CACHET-II project. Mass and energy balances for the feed side are discretized using a finite volume method. Thus, the radial profiles of temperature and chemical species concentration are determined. The sweep flow is modelled as a plug parameter.

The mass transfer across the membrane is calculated using a corrected Sieverts law, while mass transfer through the support is calculated using a Dusty Gas model. A schematic of the H_2 flux across the membrane is represented in Fig. 6.

The simulation tool accounts for:

- Bulk-phase feed side mass transfer characteristics ($P_{H_2,\text{bulk}} \rightarrow P_{H_2,\text{interface}}$).
- Permeability and mass transfer resistance associated with the membrane deposition layer ($P_{H_2,\text{interface}} \rightarrow P_{H_2,\text{wall}}$).
- Mass transfer characteristics through the ceramic support tubing ($P_{H_2,\text{wall}} \rightarrow P_{H_2,\text{support}}$).
- Bulk-phase permeate side mass transfer ($P_{H_2,\text{support}} \rightarrow P_{H_2,\text{sweep}}$).

Transport parameters are calculated as function of membrane operating conditions as temperature, pressure, velocity, etc. The mass transfer model has been validated against experimental data performed at DICP and ECN laboratories. The experimental campaign was carried out using membranes developed by DICP applying the ECN ceramic alumina supports. The result-ing parameters of the model for the pure Pd membrane are: thickness equal to 7.266×10^{-6} m, permeability at reference conditions (T = 400 °C) equal to 9.592×10^{-13} kmol m/m^2 s Pa^n, activation energy of 12.8 kJ/kmol and n equal to 0.676 (Song and Forsyth, 2013; Van Berkel et al., 2013). When a sulphur tolerant mem-brane is considered, the permeability is assumed reduced by 40% (Peters et al., 2012). With the calibrated parameters, the model showed that some parameters affect more than other the hydrogen flux. However, it can be stated that the hydrogen permeation is not affected by a single rate-limiting step mechanism, out-lining the importance of including all the hydrogen permeation resistances. This behaviour was confirmed by the sensitivity analysis performed on the main membrane parameters and shown in Fig. 7.

It can be noted that concentration polarization and mass transfer across the membrane support seem to be the two main resistances to hydrogen permeation. For further membrane development is therefore important to focus on: (i) integration of membrane into a smart module design aiming at reducing the concentration effects and (ii) decrease the support resistance for mass transport.

The same analysis was used to assess the optimal hydrogen separation configuration. The optimum configuration is composed by three membrane modules in series because of the benefit effects on the mass transfer limitation from bulk phase to membrane interface (which was found to be a critical parameter). With one and two membrane modules, the flow in the feed side is laminar type introducing significant resistances to hydrogen diffusion from bulk-to-interface of the membrane. Moving to three membrane modules, the flow becomes turbulent significantly reducing this resistance. Higher number of membranes would increase the pressure drops, hence reducing the driving force, as well as plant complexity.

6. Thermodynamic results

This section presents the thermodynamic results for the evaluated cases. Before introducing the detailed power balances, the impact of each parameter investigated on the overall efficiency, CO_2 avoidance and membrane surface area will be discussed.

6.1. Pd vs Pd-alloy membrane

The comparison between Pd and Pd-alloy membranes, which implies the use of Rectisol or Selexol as AGR, as function of HRF is shown in Fig. 8. Both cases are calculated assuming a feed gas pressure of 37 bar. It can be noted that the SPECCA variation for the two configurations is in the range of 10%: Pd membrane configuration has a lower efficiency of 0.5% percentage points because of Rectisol higher energy consumption for sulphur separation (4 MW more). The higher consumptions are partly balanced by the absence of the COS hydrolizer (Rectisol is active towards COS) avoiding the consequent thermal swing penalties. The most important difference between the two cases is in the CO_2 vented

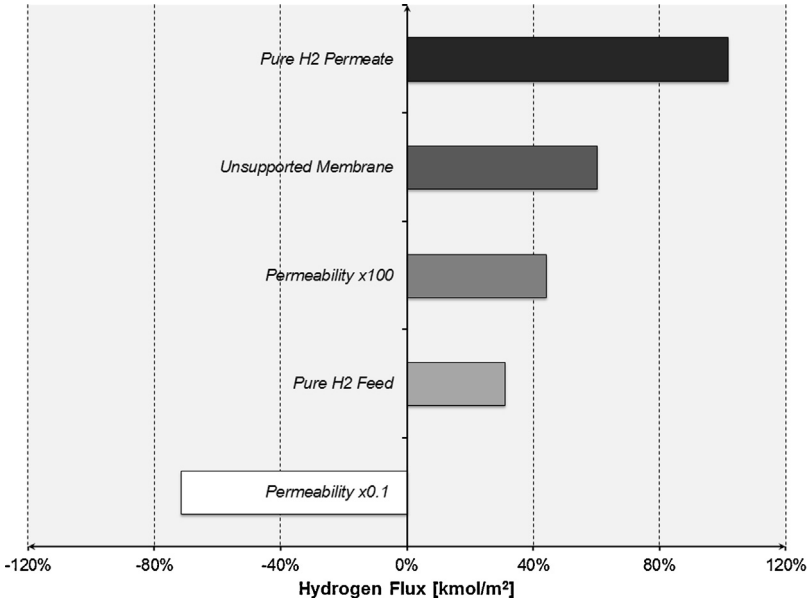

Fig. 7. Main membrane parameters influence on the hydrogen molar flux.

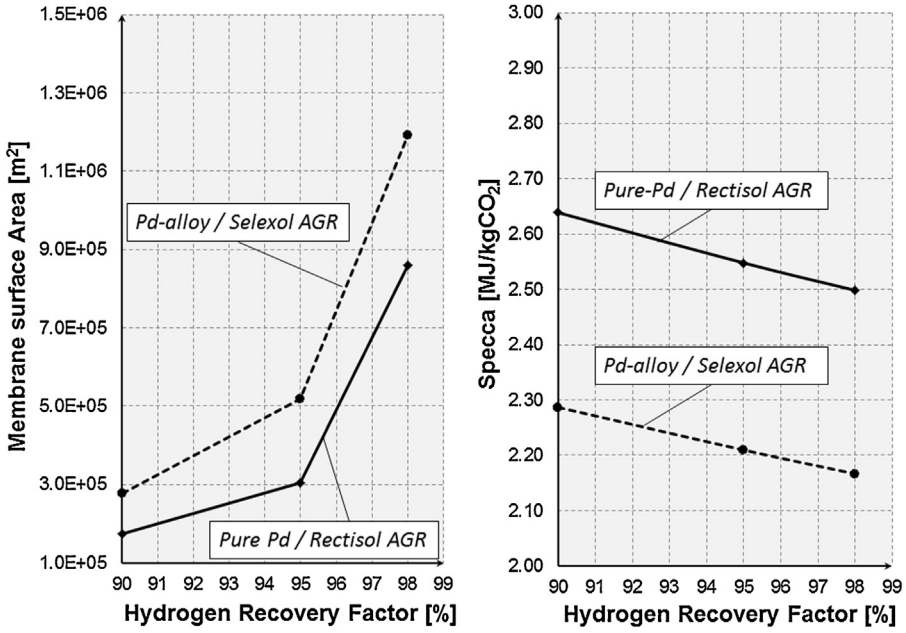

Fig. 8. Comparison between Pd (not sulfur tolerant) and Pd-alloy (low sulfur tolerant) as a function of HRF: total membrane area (left hand) and SPECCA variation (right hand).

at the AGR: Rectisol co-capture more CO_2 leading to a lower CO_2 emissions avoidance of 5%. Considering that the reference SPECCA for conventional technologies is 3.6 MJ/kg_{CO_2}, both values are promising.

On the other hand there is a significant difference in terms of membrane surface area: Pd-alloy membranes almost double the area. This is because of the lower permeance of sulfur tolerant membrane compared to the no-tolerant. Provided that membrane cost is proportional to the surface area, the Pd-alloy solution seems non-attractive when applied to conventional AGR processes. Moreover, as shown in the economic assessment, the higher capital expenditure due to the membrane area is not compensated by the lower plant cost of the Selexol process compared to the Rectisol.

6.2. HRF

The impact on HRF[2] on membrane surface area and net electric efficiency for the investigated case is shown in see Fig. 9. HRF has almost negligible impact on the plant efficiency because the hydrogen not permeated in the membrane is separated in the cryogenic process and then used in the combined cycle. On the contrary the HRF has strong impact on the membrane surface area: moving from 90% to 98%, the membrane surface area can be four times higher

[2] The HRF is the amount of hydrogen permeated across the membrane out of the maximum amount of hydrogen which can be separated.

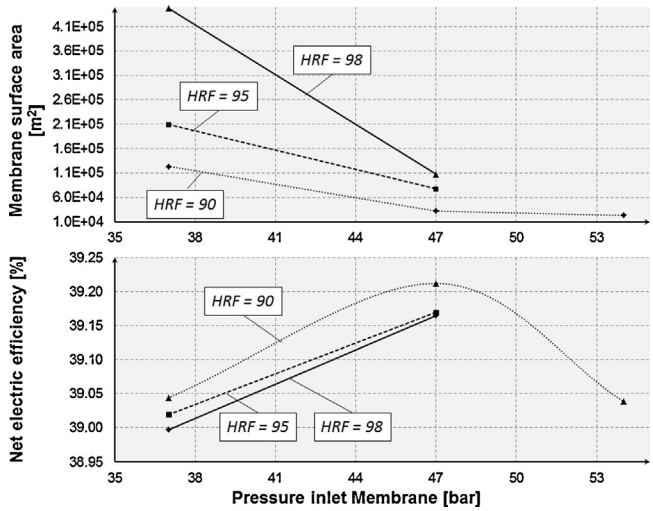

Fig. 9. Membrane surface area (top) and net electric efficiency (bottom) as function of different feed pressure and HRF (%). All cases are based on Pd/Rectisol configuration.

(i.e. for the case at 47 bar). On the CO_2 emissions, they reduce at higher HRF thanks to the higher CO_2 selectivity of the cryogenic purification process.

6.3. Feed side pressure

The feed side pressure has a significant impact on the required membrane surface area, thanks to the higher partial pressure difference between feed and permeate side. On the efficiency, the impact of feed pressure is limited: the higher compression work is partly balanced by a more efficient heat recovery of the retentate thermal power. Moreover, the steam for WGS is at 54 bar in all cases (equal to the cold RH pressure), hence there are no additional penalties from this point of view. The increase in the steam cycle power is more important than the feed compression power moving from 37 to 47 bar; this is not any longer true when the feed pressure is 54 bar. Finally, it must be stressed that the feed pressure cannot be higher than 54 bar because the CO_2 purity constraints cannot be fulfilled: the N_2 solubility in CO_2 increases with the pressure and 54 bar is the upper limit (Battino et al., 1984).

6.4. Post-firing

The main reason behind post-firing is to reduce the membrane surface area thanks to the separation of part of the hydrogen at ambient pressure. In particular, 10% of the total hydrogen separated is used to post-fire the HRSG. As drawback, the net electric efficiency should reduce.

About membrane surface area reduction, the comparison with all permeated hydrogen at 25 bar is shown in Fig. 10. Advantages of post-firing are very significant at low feed pressure (i.e. 37 bar), where the membrane surface area is more than halved; at 54 bar membrane area reduces by about 40%. The share of each membrane is also shown in Fig. 10: in all cases without post firing the last (3rd) separator shares about half of the overall surface area because of the lowest driving force. Adopting the post-firing configuration, the share of this membrane falls to almost negligible value.

6.5. Power balances

Comparing membrane plants with no capture IGCC (see Table 4), it can be noted that: (i) the thermal power input increases in order to keep the same GT dimensions, (ii) the GT power increases because of the lower LHV of the decarbonized syngas (Kim et al., 2013), (iii) the steam cycle power decreases due to the WGS steam demand, (iv) the gasifier auxiliaries and ASU consumptions raises proportionally to the fuel feedstock and (v) the nitrogen dilution compressor consumption increases because almost all the nitrogen produced is compressed and adopted as sweep gas. As far as the ref-erence capture case is concerned, the energy balances underlines the higher performance achieved by membrane plants. The electric efficiency is 3 percentage point (p.p.) higher while the CO_2 avoided varies from similar value to 5 p.p. lower depending on the feed pressure and HRF (the lower the HRF the lower the CO_2 recovered). The resulting SPECCA is in the range of 2.3–2.6 MJ/kg_{CO_2}, significantly lower than reference Selexol capture.

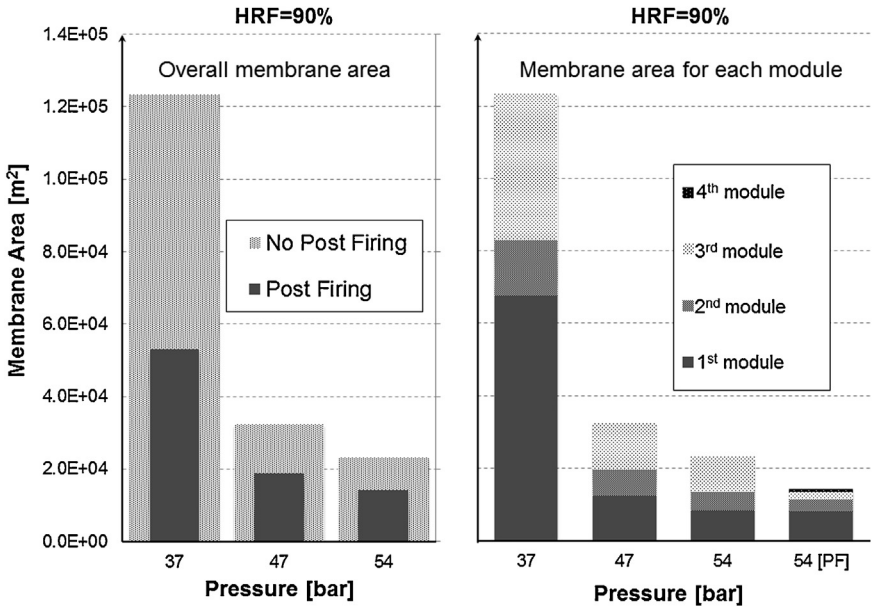

Fig. 10. Membrane surface area for different feed pressure and HRF = 90%. On the left side the overall membrane area comparison between layout without post firing (light grey) and with post firing (dark grey). On the right side the membrane area for each module is shown for cases with different feed pressure: 37, 47 and 54 bar for the plant without post firing and 54 bar when post firing is adopted.

Table 4
Power balances for the investigated cases and two reference cases.

	IGCC no cap	IGCC Selexol cap	Pd-alloy[a] membrane	Pd[a] membrane (*not sulfur tolerant*)					PF
				No post-firing					
HRF, %	–	–	90	90	90	95	98	90	90
Feed pressure, bar	–	–	36.4	36.4	47	47	47	54	54
Gas turbine, MW	290.2	305.0	331.6	332.2	323.5	327.2	329.2	323.1	315.8
Steam cycle gross/Aux, MW	197.7	179.2	168.2	169.8	173.8	170.9	169.1	174.2	223.2
Expander ASU, MW	8.5	10.2	9.9	9.9	9.8	9.8	9.8	9.8	10.6
HRSC pumps, MW	3.1	3.2	2.9	2.9	3.1	3.1	3.0	3.1	3.8
Coal handling, MW	1.7	1.9	1.9	1.9	1.9	1.9	1.9	1.9	2.1
Ash handling, MW	0.5	0.6	0.6	0.6	0.6	0.6	0.6	0.6	0.6
Sulphur absorption, MW	0.4	19.3	0.4	4.6	4.5	4.5	4.5	4.5	4.9
Lock hopper compressor, MW	9.2	11.1	12.1	12.2	12.0	12.0	12.0	12.0	13.0
Sweep compressor, MW	32.1	24.0	39.2	39.5	38.8	39.0	39.0	38.9	41.7
ASU + O_2 compressor, MW	22.7	26.6	26.2	26.4	26.0	26.1	26.1	26.0	28.2
Gasifier blower, MW	1.1	1.3	1.2	1.2	1.2	1.2	1.2	1.2	1.3
CO_2 compressor, MW	–	22.9	10.6	10.7	9.9	9.6	9.5	9.6	10.2
Feed compressor, MW	–	–	0.0	0.0	2.2	2.2	2.2	4.0	4.5
Heat rejections, MW	2.5	2.5	2.2	2.2	2.3	2.3	2.2	2.4	2.8
BOP, MW	0.7	1.3	2.0	2.0	1.2	1.3	1.4	1.2	1.1
Net power output, MW	422.4		410.3	407.7	403.2	404.1	404.4	401.7	435.42
Thermal power input, MW	896.6	1044.4	1037.1	1044.1	1028.3	1031.6	1032.6	1028.9	1104.4
Efficiency, %	47.12	36.00	39.57	39.04	39.21	39.17	39.16	39.04	39.09
Specific emission, g/kWh	732.1	98.50	94.5	130.4	114.3	98.8	89.4	104.5	104.42
CO_2 avoided, %	–	87.00	87.1	82.2	84.4	86.5	87.8	85.7	85.74
SPECCA, MJ/kg_{CO_2}	–	3.72	2.29	2.62	2.49	2.45	2.41	2.52	2.50
Membrane area, m^2	–	–	233,508	123,458	32,486	77,648	107,075	23,268	14,297

[a] Pd-alloy membranes are slightly sulfur tolerant and adopt SELEXOL as process sulfur removal process.

Also for different HRF, the gas turbine power output reflects the LHV of the fuel entering the gas turbine: the lower the LHV the higher the GT power. Nevertheless, this effect is not straightforward because of the mixing of the gas recycled from the cryogenic process to the hydrogen permeated. At higher HRF the recycled gas contains less H_2 and more CO_2 resulting in a lower LHV. As far as the steam cycle power output is concerned, it reduces at higher HRF due to the lower heat available after membrane modules. Other consumptions do not feature significant differences. Auxiliaries consumptions are almost constant among the different membrane cases but for the feed compressor. Provided the similar power balances at different HRF or feed pressure, the SPECCA results to be primarily affected by the amount of CO_2 avoided and therefore by the cryogenic separation efficiency. High HRF and high feed pressure increase the CO_2 recovery.

As shown in Table 5, different post firing configurations can be considered. The first parameter which can be modified is the maximum steam temperature achieved in the HRSG. Increasing the temperature from the value of 565–585 °C (state-of-the-art, H class combined cycle) the electric efficiency increases of about 0.3 percentage point with no consequences on other working conditions. This results in a lower SPECCA with equal membrane surface area. Increasing the steam temperature up to 620 °C, typical value of USC plants, the efficiency reaches 39.6%, reducing the SPECCA down to 2.3 MJ/kg_{CO_2}. Thanks to the advantages of the post firing layout, solutions which were no convenient in the reference configuration become now more interesting: (i) the feed pressure can be reduced to 47 bar with limited membrane area increase and (ii) the HRF can be increased up to 95% at 47 bar with only 10% rise of the membrane area (without post-firing it was more than 100%). The economic assessment will indicate which membrane operating minimizes the cost of CO_2 avoided.

6.6. HRSG temperature profile

Provided the complex heat management in a pre-combustion IGCC plant, the evaluation of all the modifications caused by HRSC post firing is very challenging. On the other hand, a straightforward analysis can be carried out considering only the heat recovery steam generator and the gas/steam heat exchange. Accordingly, Fig. 11 shows the temperature-heat duty diagram for cases with and without post firing (PF). Comparing the no PF with the PF configuration it can be firstly noted an increase in the heat exchanged of about 20% thanks to the hydrogen oxidation with an overall increase of steam production. The minimum temperature difference between flue gas and water (ΔT_{pp}) moves from the HP evaporator towards the HP economization section. No LP steam generation takes place inside the HRSG when post firing is applied. On the other hand, the

Table 5
Power balances for the cases post-firing configuration at different HRF, feed pressure and maximum steam temperature in the HRSG.

	PF1	PF2	PF3	PF4	PF5	PF6
HRF, %	90	90	90	90	90	95
Feed pressure, bar	54	54	54	37	47	47
T_{max} steam HRSC, °C	565	585	620	565	565	565
H_2 sent to PF, % of total sep	10	10	10	10	10	10
Net power output, MW	435.42	437.09	439.90	439.32	442.16	438.65
Efficiency, %	39.09	39.27	39.59	39.55	39.75	39.12
CO_2 avoided, %	85.74	85.78	85.86	82.42	86.66	86.49
SPECCA, MJ/kg_{CO_2}	2.50	2.43	2.31	2.42	2.23	2.47
Membrane area, m^2	14,297	14,297	14,297	53,223	18,827	21,425

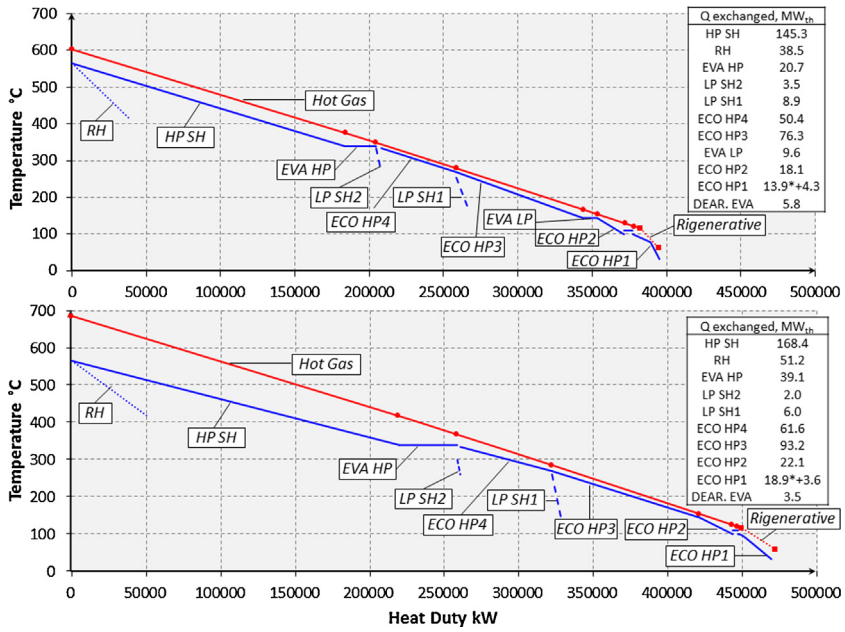

Fig. 11. Temperature-heat duty diagram of the heat recovery steam generator. (a) HRSG without post firing and (b) HRSG with post firing. Maximum steam temperature is limited to 565 in both cases. Regenerative heating is based on steam turbine bleedings.

amount of HP steam production increases becoming the only relevant pressure level of the steam cycle. Consistently, the amount of heat exchanged at high temperature (which means higher than T_{EVA_HP}) compared to the total heat released by the flue gases rises from 53.5% to 57.5%. This means that the available energy is better harnessed. On the other hand the area between the flue gas and the steam along the HP super-heaters broaden, increasing the exergy losses due to finite temperature heat exchange. Eventually, thanks to the larger amount of energy available for HP steam SH and RH, more HP steam can be produced outside and inside the HRSG; this results in an increase of the turbine power output compared to the heat available in the flue gases: from 174 MW to 223 MW. The efficiency gain is even more relevant when higher maximum steam temperature (585 or 620) is considered. Such an increase allows narrowing the temperature difference along the SH/RH section, lowering the heat transfer losses. Therefore, the adoption of ambient pressure hydrogen separation does not imply significant changes in the plant efficiency. Indeed, the hydrogen oxidation is better harnessed when the maximum steam temperature is increased.

7. Economic assessment

The economic assessment is based on the methodology proposed by EBTF (Franco et al., 2011, 2010). This methodology neglects transport and storage costs as not of interest when different capture techniques are compared and no specific area is considered. Reference values for transport and storage cost are reported in ("Global CCS Institute," n.d., 2011) ranges between 1.5 and 16 €/t_{CO_2} for transport and 2–20 €/t_{CO_2} for storage. The

Table 6
Equipment cost references for main components.

Plant component	Scaling parameter	Reference erected cost C_0 (M€)	Reference size, S_0	Scale factor	N
Gasification section					
Coal handling[a,b]	Coal input, kg/s	27.5	32.9	0.67	1
Ash handling[a,b]	Ash flow rate, kg/s	4.7	9.7	0.6	1
Gasifier[a,b]	Thermal input, MW	90.0	828.0	0.67	1
Air separation unit (ASU)[a,b]	Oxygen produced, kg/s	26.6	28.9	0.7	1
Power section					
Gas turbine, generator and auxiliaries[a,b,c]	$GT_{Net\ Power}$, MW	49.4	272.12	0.3	1
HRSG, ducting and stack[a,b,c]	U*S, MW/K	32.6	12.9	0.67	1
Steam turbine, generator and auxiliaries[a,b,c]	$ST_{Gross\ power}$, MW	33.7	200.0	0.67	1
Cooling water system and BOP[a,b,c] Nitrogen	Q_rejected, MW	49.6	470.0	0.67	1
compressor for GT dilution [b]	Compressor power, MW	14.8	47.6	0.67	1
Gas conditioning and CO_2 separation section					
Low temperature heat recovery (LTHR)[a,b]	Thermal input, MW	6.1	828.0	0.67	1
Selexol acid gas removal (AGR)[a,b]	Coal input, kg/s	12.0	32.9	0.67	1
Rectisol Acid gas removal (AGR)[a,b]	Coal input, kg/s	13.2	32.9	0.67	1
Water treatment [b]	Coal input, kg/s	10.7	32.9	0.67	1
Claus[b]	Sulphur flow rate, kg/s	8.0	0.2	0.67	1
Water gas shift reactors[b]	Thermal input, MW	11.7	954.1	0.67	2
Selexol CO_2 separation system[a,b]	CO_2 captured, kg/s	28.1	69.4	0.8	1
CO_2 compressor and condenser[a,b]	Compressor power, MW	9.9	13.0	0.67	1

[a] DOE/NETL-2011/1498 (n.d.).
[b] Franco et al. (2011, 2010).
[c] "Gas Turbine World Handbook," (2010).

Table 7
O&M and consumable costs (PH3/14, n.d.; PH4/33, n.d.).

Coal Costs	€/GJ_{LHV}	3
O&M		
Labour costs for IGCC cases	M€	8.9
Maintenance	% of total plant cost	1
Insurance	% of total plant cost	1
Consumables		
Evaporative tower blow-off	% of evaporated water	100
Cooling water make-up costs	€/m^3	0.35
HRSG water blow-off	% of steam produced	1
Process water costs	€/m^3	2
Rectisol	% Equipment cost	2
Catalyst replacement		
Water gas shift lifetime	Years	5
Water gas shift cost	k€/m^3	14
Membrane tubes replacement		
Membrane tube lifetime	Years	5

variation depends on the power plant distance from the storage site, the transportation technology and the type of storage assumed.

The cost of electricity (COE) is calculated from adopted IEA models by setting the net present value (NPV) of the power plant to zero (PH3/14, n.d.; PH4/33, n.d.). This can be achieved by varying the plant COE until the revenues balance the cost over the whole life time of the power plant.

Total plant costs are calculated with the Bottom-Up Approach (BUA). This approach is the most typical for innovative plant where no construction experience exists.

The first step consists of calculating total direct plant cost (TDPC) from equipment costs and then adding installation costs such as piping, erection, outside battery limits (OBL), etc. Total direct plant costs plus indirect costs (IC), which are calculated as a percentage of direct plant costs, lead to engineering, procurement and construction costs (EPC). Finally, total plant cost (TPC) results from EPC plus owner's cost and contingencies.

The equipment cost database is summarized in Table 6. Most of the other data used for the gasification island are taken from (Franco et al., 2011, 2010) which are consistent with (DOE/NETL-2011/1498, n.d.). About power section, GT specific costs are calculated as an average of F-Class gas turbine ("Gas Turbine World Handbook," 2010). A constant mass flow rate at turbine outlet is assumed for all cases, which therefore have the same size but for the generator power output; this results in a low scale factor of 0.3. Combustor modifications required by syngas combustion are not taken into account due to the difficult in predicting correct figures.

Rectisol and Selexol cost evaluation was assessed with a bottom-up approach, starting from the data presented in (Doctor et al., 1996) and carrying out a preliminary sizing of each process component. For a defined quality of coal feedstock, the AGR cost is scaled using the amount of coal treated (or the thermal power input).

Membrane module costs of 5800 €/m^2were determined in CACHET-II project (Song and Forsyth, 2013) with no scaling fac-tor as consequence of their modularity. They are based on a design with 19 membrane tubes for a total surface area for each module of about ten square metres as proposed by Technip within CACHET-II project (Song and Forsyth, 2013). Costs include membrane tubes, sealings, vessel materials and manufacturing. The membranes and sealing costs shares about 35% of the overall module costs. Lifetime of membrane tubes is equal to five years, while the membrane vessel itself is assumed to be recycled; the cost of the membrane tubes replacement is accounted as consumable cost. Additional costs for

Table 8
Component costs, total equipment cost, total plant cost and specific investment costs for the main considered cases. Costs are in M€.

HRF, %	No post-firing					Post-firing	
	90			95	98	90/565 °C	90/620 °C
Feed pressure, bar	37	47	54	47	47	54	54
Coal handling	30.6	30.3	30.3	30.4	30.4	32.0	31.9
Gasifier	104.5	103.5	103.5	103.7	103.8	109.2	109.0
Gas turbine	52.4	52.0	52.0	52.2	52.3	51.7	51.6
Steam turbine	30.2	30.7	30.7	30.3	30.1	36.3	36.8
HRSG	38.1	38.1	38.1	38.1	38.1	39.2	52.3
LTHR	7.1	7.0	7.0	7.0	7.0	7.4	7.4
Heat rejection	34.8	36.1	36.2	35.5	35.1	40.6	40.2
ASU	34.3	33.9	33.9	34.0	34.0	35.9	35.8
ASH	11.1	11.0	11.0	11.0	11.0	11.5	11.5
AGR	15.0	14.9	14.9	14.9	14.9	15.7	15.7
Gas cleaning	4.5	4.4	4.4	4.4	4.4	4.7	4.7
Water treatment	11.9	11.8	11.8	11.8	11.8	12.4	12.4
Claus	9.6	9.5	9.5	9.6	9.6	10.1	10.1
CO_2 compressor	8.7	8.3	8.1	8.1	8.1	8.5	8.4
Membrane	716.1	188.4	135.0	450.5	621.0	82.9	82.9
Sweep compression	12.8	12.7	12.7	12.8	12.8	16.2	16.2
Saturator	0.2	0.2	0.2	0.2	0.2	0.2	0.2
HTS	4.3	4.2	4.2	4.2	4.2	4.5	4.5
Air expander	5.7	5.6	5.6	5.6	5.6	6.8	6.8
Cryogenic	0.9	0.8	0.8	0.8	0.8	0.9	0.9
LT heat exchangers	3.5	3.5	3.5	3.5	3.5	3.5	3.5
HT heat exchangers	8.5	8.5	8.5	8.5	8.5	8.5	8.5
Total equipment cost	1144.7	615.4	562.0	877.0	1047.1	538.3	550.9
Total plant cost	2701.2	1452.2	1326.2	2069.5	2471.0	1270.2	1300.1
Net power output, MW	407.7	403.2	401.7	404.1	404.4	435.4	439.9
Net Electric efficiency, %	39.0	39.2	39.0	39.2	39.2	39.1	39.6
CO_2 avoided, %	85.0	84.4	85.7	86.5	87.8	85.7	85.9
Specific costs, €/kW_{gross}	5276.8	2864.3	2615.4	4075.2	4862.3	2311.3	2348.7
Specific costs, €/kW_{net}	6625.9	3601.5	3301.6	5121.9	6109.9	2917.1	2955.5

Table 9
Comparison between membrane cases and reference cases in terms of cost of electricity and cost of CO_2 avoided. Total COE is subdivided into four main voices: investment, fixed O&M, consumables and fuels.

	IGCC No cap	IGCC Selexol	Membrane No post firing	Membrane With post firing			
HRF, %	–	–	90	90	95	90	90
Feed pressure, bar	–	–	54	47	47	54	54
T_{max} steam [°C]	565	565	565	565	565	565	620
Investment cost, [€/MWh]	34.51	47.46	52.3	50.3	51.3	48.0	48.6
Fixed O&M costs, [€/MWh]	7.07	8.99	9.4	8.9	9.1	8.7	8.7
Consumables, [€/MWh]	1.82	3.14	5.5	5.1	5.5	4.7	4.6
Fuel costs, [€/MWh]	22.92	29.97	27.7	27.2	27.6	27.6	27.3
COE, [€/MWh]	66.32	89.55	95.0	91.5	93.5	89.0	89.2
Cost of CO_2 avoided [€/t_{CO_2}]	–	36.7	45.6	39.7	42.9	36.1	36.5

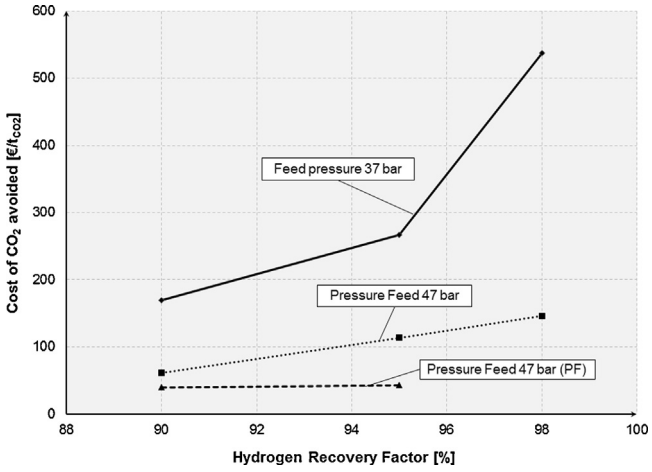

Fig. 12. Cost of CO_2 avoided as function of the hydrogen recovery factor for different feed pressure (37 or 47) and different layout (without and with post firing).

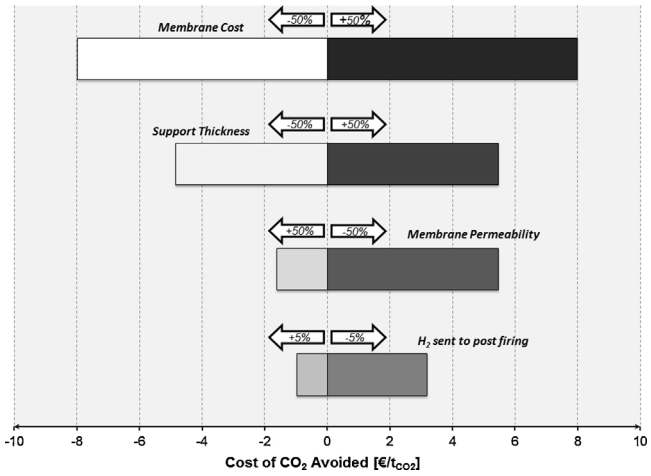

Fig. 13. Cost of CO_2 avoided for 50% increase or decrease of: (i) membrane module cost, (ii) support thickness, (iii) membrane permeability and (iv) hydrogen burned in the HRSG.

post-firing are neglected because of the low pressure and limited power.

About O&M costs, the IEA methodology[3] was adopted assuming coefficient calibrated towards EBTF figures. The details for O&M figures are reported in Table 7. Labour costs refer to an average European social environment.

8. Economic results

Equipment and total plant costs for the most interesting scenarios are summarized in Table 8. Results of the case without post firing are reported in term of different HRF (90, 95 and 98%) and feed pressure (37, 47 and 54 bar). The presented post firing configurations differ only for the steam cycle maximum temperature which primarily affects the HRSG costs. Among the seven cases shown, equipment costs are similar but the membrane modules which range from 82 M€ to 716 M€. The large variation of the mem-brane module cost was expected since it is proportional to the membrane surface area as shown before. Consistently, it is interesting to compare the cost share of membrane on the entire power plant: in post-firing cases, the membrane cost share is 15%, therefore significant and even higher than GT. Without post-firing, the membrane cost share steeply increases, varying from 25% to 55%. The significant impact of membrane costs on the overall plant leads the specific costs to more than 3300 €/kW for cases without post-firing and slightly lower than 3000 €/kW for post-firing cases (the specific costs for the reference IGCC without capture is equal to 2100 €/kW, while with capture is 2900 €/kW (Franco et al., 2011)).

It can be noted that membrane cases are penalized compared to the reference case from the specific plant cost point of view.

The cost of CO_2 avoided for membrane cases is shown in Fig. 12; most promising cases are also reported in Table 9. All cases without post firing feature a cost of CO_2 avoided higher than 45 €/t_{CO_2}, which is significantly higher than the reference Selexol case (36 €/t_{CO_2}). The high cost of CO_2 avoided is mainly due to the higher investment costs (+5 €/MWh) as well as membrane substitution every five years (+2.2 €/MWh). The increase of the feed pressure positively affects the CO_2 capture cost, most of all at high HRF without post-firing. The membrane driving force at 47 bar and 98 HRF is high enough to avoid the steep cost increase registered at 37 bar, 98 HRF. Looking at the post-firing cases results, the cost of CO_2 avoided decreases to 36 €/t_{CO_2} thanks to the membrane surface area reduction. Compared to the Selexol CO_2-capture plant, the higher investment costs are balanced by the lower fuel consumptions. This is a promising result which makes the post-firing configuration very attractive. Another important result is that the cost of CO_2 avoided in PF cases is very close between 90% and 95% of HRF. Finally, the cost of CO_2 avoided is equal between the cases with maximum steam temperature of 565 °C and 620 °C: the higher performances of 620 °C are balanced by the lower costs for 565 °C case (20% increase of the HRSG cost has been assumed for 620 °C). Eventually, a sensitivity analysis on membrane performances and costs was performed in order to determine the most important parameter affecting the cost of CO_2 avoided. This analysis is performed on the most promising configuration: the PF case with

[3] The IEA methodology assumes that fixed costs as maintenance and insurance are function of the total plant costs.

90% HRF and feed pressure of 54 bar. Four parameters were varied by ±50%: membrane costs, support thickness, membrane permeability and H_2 sent to PF. As shown in Fig. 13, the membrane cost reduction is the aspect where research activity should focus on. It must be outlined that this reduction can be achieved by changing the module design and increasing the number of membrane tubes per module, thereby increasing the membrane area amount installed per vessel.

9. Conclusions

This work discussed the application of hydrogen selective membranes to Integrated Gasification combined Cycle for CO_2 capture. The membrane tubes and membrane modules performances as well the costs adopted for the assessment were developed within CACHET-II project.

Compared to previous works, a detailed thermodynamic and economic assessment of plant integrating membranes for H_2 separation is performed. Moreover, the membrane area is assessed with a detailed model developed within the project.

A first lay-out was calculated where all the hydrogen is separated at high pressure to feed the gas turbine. This configuration features very high performances but also costs, because of the large membrane surface area requirements. A second innovative lay-out was presented where part of the hydrogen is separated at low pressure to feed the post firing of the heat recovery steam generator. This innovative lay-out preserves the efficiency of the previous lay-out while cutting down the membrane surface area and matching the cost of CO_2 avoided of the reference IGCC with CO_2 capture. A sensitivity analysis showed that the cost reduction of the module is the key for further economic improvement. As far as the membranes developed within CACHET-II project are concerned and considering only the separator performances, the membrane support rather than the permeability seems to be the key parameter to focus on in order to improve the hydrogen flux.

Acknowledgements

The CACHET-II project has received funding from the European Community's Seventh Framework Programme FP7/2007–2013 under grant agreement n° 241342.

References

Amrollahi, Z., Ertesvåg, I.S., Bolland, O., 2011. Optimized process configurations of post-combustion CO_2 capture for natural-gas-fired power plant—exergy analysis. International Journal of Greenhouse Gas Control 5, 1393–1405, http://dx.doi.org/10.1016/j.ijggc.2011.09.004.

Anantharaman, R., Bolland, O., 2011. Integration of oxygen transport membranes in an IGCC power plant with CO_2 capture. Chemical Engineering Transactions 25, 25–30.

Battino, R., Rettich, T., Toshihiro, T., 1984. Solubility of nitrogen and air in liquids. Journal of Physical and Chemical Reference Data 13, 567–600.

Beavis, R., 2011. The EU FP6 CACHET project – final results. Energy Procedia 4, 1074–1081, http://dx.doi.org/10.1016/j.egypro.2011.01.157.

Berstad, D., Anantharaman, R., Nekså, P., 2013. Low-temperature CO_2 capture technologies – applications and potential. International Journal of Refrigeration 36, 1403–1416, http://dx.doi.org/10.1016/j.ijrefrig.2013.03.017.

Bredesen, R., Jordal, K., Bolland, O., 2004. High-temperature membranes in power generation with CO_2 capture. Chemical Engineering and Processing: Process Intensification 43, 1129–1158, http://dx.doi.org/10.1016/j.cep.2003.11.011.

Campanari, S., Chiesa, P., Manzolini, G., 2010. CO_2 capture from combined cycles integrated with Molten Carbonate Fuel Cells. International Journal of Greenhouse Gas Control 4, 441–451, http://dx.doi.org/10.1016/j.ijggc.2009.11.007.

Casas, N., Schell, J., Joss, L., Blom, R., Mazzotti, M., 2012. A novel adsorbent material (MOF/MCM-41) for pre-combustion CO_2 capture by pressure swing adsorption. In: GHGT-11 Conference Proceedings. 19–23 November 2012, Kyoto.

Chiesa, P., Campanari, S., Manzolini, G., 2011. CO2 cryogenic separation from combined cycles integrated with molten carbonate fuel cells. International Journal of Hydrogen Energy 36, 10355–10365, http://dx.doi.org/10.1016/j.ijhydene.2010.09.068.

Chiesa, P., Kreutz, T.G., Lozza, G.G., 2007. CO_2 sequestration from IGCC power plants by means of metallic membranes. Journal of Engineering for Gas Turbines and Power 129, 123, http://dx.doi.org/10.1115/1.2181184.

Chiesa, P., Macchi, E., 2004. A thermodynamic analysis of different options to break 60% electric efficiency in combined cycle power plants. Journal of Engineering for Gas Turbines and Power 126, 770, http://dx.doi.org/10.1115/1.1771684.

De Lorenzo, L., Kreutz, T.G., Chiesa, P., Williams, R.H., 2008. Carbon-free hydrogen and electricity from coal: options for syngas cooling in systems using a hydrogen separation membrane reactor. Journal of Engineering for Gas Turbines and Power 130, 031401, http://dx.doi.org/10.1115/1.2795763.

Dijk, E. Van, Walspurger, S., Cobden, P., Brink, R. Van Den, 2011. Testing of hydrotalcite based sorbents for CO_2 and H_2S capture for use in sorption enhanced water gas shift. International Journal of Greenhouse Gas Control 5, 505–511.

Doctor, R., Molburg, J., Thimmapuram, P., 1996. Oxygen-Blow Gasification Combined Cycle: Carbon Dioxide, Recovery, Transport, and Disposal.

DOE, 2007. Carbon Sequestration Technology Roadmap and Program Plan.

DOE/NETL, 2011/1498, n.d. Cost and Performance of PC and IGCC Plants for a Range of Carbon Dioxide Capture.

Franco, F., Anantharaman, R., Bolland, O., Booth, N., Dorst, E., Van Ekstrom, C., 2010. Common framework and test cases for transparent and comparable techno-economic evaluations of CO_2 capture technologies – the work of the European Benchmarking Task Force. Energy Procedia, 1–8.

Franco, F., Anantharaman, R., Bolland, O., Booth, N., Dorst, E. Van, Ekstrom, C., 2011. European best practice guide for assessment of CO_2 capture technologies. Gas Turbine World Handbook, 2010.

Gazzani, M., Macchi, E., Manzolini, G., 2013a. CO_2 capture in integrated gasification combined cycle with SEWGS – Part A: thermodynamic performances. Fuel 105, 206–219, http://dx.doi.org/10.1016/j.fuel.2012.07.048.

Gazzani, M., Manzolini, G., Macchi, E., Ghoniem, A., 2013b. Reduced order modeling of the Shell-Prenflo entrained flow gasifier. Fuel 104, 822–837, http://dx.doi.org/10.1016/j.fuel.2012.06.117.

Global CCS Institute [WWW Document], n.d., 2011. The Cost of CO_2 Capture, Transport and Storage. http://www.globalccsinstitute.com/sites/default/files/eco-assess-ccs-tech-2010-4b.pdf

Grabner, M., Meyer, B., 2013. Performance and exergy analysis of the current developments in coal gasification technology. Fuel, http://dx.doi.org/10.1016/j.fuel.2013.02.045.

Guazzone, F., Ma, Y.H., 2008. Leak growth mechanism in composite Pd membranes prepared by the electroless deposition method. AIChE Journal 54, 487–494.

Guo, X., Lu, W., Zhenghua, D., Liu, H., Gong, X., Li, L., Honglin, Z., Guo, B., 2012. Experimental investigation into a pilot-scale entrained-flow gasification of pulverized coal using CO_2 as carrier gas. Energy & Fuels 26, 1063–1069.

Higman, C., van der Burgt, M., 2008. Gasification. Elsevier.

International Energy Agency, 2008. CO_2 Capture and Storage – A Key Carbon Abatement Option.

Jordal, K., Bredesen, R., Kvamsdal, H.M., Bolland, O., 2004. Integration of H_2-separating membrane technology in gas turbine processes for CO_2 capture. Energy 29, 1269–1278, http://dx.doi.org/10.1016/j.energy.2004.03.086.

Kim, S., Park, S., Lee, J., Kang, D., Kim, T., 2013. Analysis of the impact of gas turbine modifications in integrated gasification combined cycle power plants. Energy 55, 977–986, http://dx.doi.org/10.1016/j.energy.2013.03.041.

Korens, N., Simbeck, D.R., Wilhelm, D.J., 2002. Process Screening Analysis of Alternative Gas Treating and Sulfur Removal for Gasification. Mountain View, CA, USA.

Ku, A.Y., Kulkarni, P., Shisler, R., Wei, W., 2011. Membrane performance requirements for carbon dioxide capture using hydrogen-selective membranes in integrated gasification combined cycle (IGCC) power plants. Journal of Membrane Science 367, 233–239, http://dx.doi.org/10.1016/j.memsci.2010.10.066.

Lee, C., Lee, S., Park, J., Lee, D., Hwang, K., Ryi, S., Kim, S., 2013. Long-term CO_2 capture tests of Pd-based composite membranes with module configuration. International Journal of Hydrogen Energy 38, 7896–7903, http://dx.doi.org/10.1016/j.ijhydene.2013.04.053.

Lozza, G., 1990. Bottoming Steam Cycles for Combined Gas-Steam Power Plants: A Theoretical Estimation of Steam Turbine Performance and Cycle Analysis. ASME Cogen-Turbo, New Orleans.

Macchi, E., Consonni, S., Lozza, G., Chiesa, P., 1995. An assessment of the thermodynamic performance of mixed gas-steam cycles. A intercooled and steam-injected cycles. Journal of Engineering for Gas Turbines and Power Transactions of the ASME 117, 489–498.

Manzolini, G., Campanari, S., Chiesa, P., Giannotti, a., Bedont, P., Parodi, F., 2012a. CO_2 separation from combined cycles using Molten carbonate fuel cells. Journal of Fuel Cell Science and Technology 9, 011018, http://dx.doi.org/10.1115/1.4005125.

Manzolini, G., Giuffrida, A., Gazzani, M., Macchi, E., Doukelis, A., Koumanakos, A., Panopolous, K., Atsonios, K., 2011. CACHET-2 Project: D4.2 Base Case Report.

Manzolini, G., Macchi, E., Gazzani, M., 2012b. CO_2 capture in natural gas combined cycle with SEWGS, Part B: economic assessment. International Journal of Greenhouse Gas Control 12, 502–509, http://dx.doi.org/10.1016/j.ijggc.2012.06.021.

Manzolini, G., Macchi, E., Gazzani, M., 2013. CO_2 capture in integrated gasification combined cycle with SEWGS – Part B: economic assessment. Fuel 105, 220–227, http://dx.doi.org/10.1016/j.fuel.2012.07.043.

Martinez, I., Grasa, G., Murillo, R., Arias, B., Abanades, J., 2013. Modelling the continuous calcination of $CaCO_3$ in a Ca-looping system. Chemical Engineering Journal 215–216, 174–181, http://dx.doi.org/10.1016/j.cej.2012.09.134.

Mejdell, A.L., Peters, T.A., Stange, M., Venvik, H.J., Bredesen, R., 2009. Performance and application of thin Pd-alloy hydrogen separation membranes in different

configurations. Journal of the Taiwan Institute of Chemical Engineers 40, 253–259, http://dx.doi.org/10.1016/j.memsci.2010.01.012.

Middleton, P., Hurst, P., Walker, G., 2005. GRACE non-integrated reactor/module concept. In: Thomas, D. (Ed.), Carbon Dioxide Capture for Storage in Deep Geological Formations—Results from the CO2 Capture Project; Capture and Separation of Carbon Dioxide from Combustion Sources. Elsevier, Naperville.

Nord, L.O., Anantharaman, R., Bolland, O., 2009. Design and off-design analyses of a pre-combustion CO_2 capture process in a natural gas combined cycle power plant. International Journal of Greenhouse Gas Control 3, 385–392, http://dx.doi.org/10.1016/j.ijggc.2009.02.001.

Peters, T., Tucho, W.M., Ramachandran, A., Stange, M., Walmsley, J., Holmestad, R., Borg, A., Bredesen, R., 2009. Thin Pd–23%Ag/stainless steel composite membranes: long-term stability, life-time estimation and post-process characterisation. Journal of Membrane Science 326, 572–581, http://dx.doi.org/10.1016/j.memsci.2008.10.053.

Peters, T.A., Kaleta, T., Stange, M., Bredesen, R., 2012. Inhibition of hydrogen transport through a selection of thin Pd-alloy membranes by H_2S: membrane stability and flux recovery in H_2/N_2 and WGS feed mixtures. Catalysis Today, 8–19.

PH3/14. I. report, n.d. Leading options for the capture of CO_2 emissions at power stations.

PH4/33. I. report, n.d, Improvment in power generation with post-combustion capture of CO_2.

Rao, A., Rubin, E., 2002. A technical economic and environmental assessment of amine-based CO_2 capture technology for power plant greenhouse gas control. Environmental Technology 36, 4467–4475, http://dx.doi.org/10.1021/es0158861.

Riberiro, R., Grande, C., Rodrigues, A., 2012. Electrothermal performance of an activated carbon honeycomb monolith. Chemical Engineering Research and Design 90, 2013–2022.

Romano, M., Chiesa, P., Lozza, G., 2010. Pre-combustion CO_2 capture from natural gas power plants, with ATR and MDEA processes. International Journal of Greenhouse Gas Control 4, 785–797, http://dx.doi.org/10.1016/j.ijggc.2010.04.015.

Schell, J., Casas, N., Marx, D., Blom, R., Mazzotti, M., 2013. Comparison of commercial and new adsorbent materials for precombustion CO_2 capture by pressure swing adsorption. In: GHGT-11 Conference Proceedings. 19–23 November 2012, Kyoto.

Schiebahn, S., Riensche, E., Weber, M., Stolten, D., 2012. Integration of H_2-selective membrane reactors in the integrated gasification combined cycle for CO_2 separation. Chemical Engineering & Technology 35, 555–560, http://dx.doi.org/10.1002/ceat.201100497.

Scholes, C.A., Smith, K.H., Kentish, S.E., Stevens, G.W., 2010. CO_2 capture from pre-combustion processes—strategies for membrane gas separation. International Journal of Greenhouse Gas Control 4, 739–755, http://dx.doi.org/10.1016/j.ijggc.2010.04.001.

Song, B., Forsyth, J., 2013. Cachet II: carbon capture and hydrogen production with membranes. Energy Procedia.

Valenti, G., Bonalumi, D., Macchi, E., 2012. A parametric investigation of the chilled ammonia process from energy and economic perspectives. Fuel 101, 74–83, http://dx.doi.org/10.1016/j.fuel.2011.06.035.

Van Berkel, F., Hao, C., Bao, C., Jiang, C., Xu, H., Morud, J., Peters, T., Soutif, E., Jansen, D., Song, B., 2013. Pd-membranes on their way towards application for CO_2 capture. Energy Procedia, 2.

Wang, M., Lawal, A., Stephenson, P., Sidders, J.C.R., 2011. Post-combustion CO_2 capture with chemical absorption: a state-of-the-art review. Chemical Engineering Research and Design 89, 1609–1624, http://dx.doi.org/10.1016/j.cherd.2010.11.005.

White, V., Torrente-Murciano, L., Sturgeon, D., Chadwick, D., 2010. Purification of oxyfuel-derived CO_2. International Journal of Greenhouse Gas Control 4, 137–142.